

Characteristics of solar-like oscillations of secondary red clump stars

Wuming Yang^{1,2*}, Xiangcun Meng¹, Shaolan Bi², Zhijia Tian², Kang Liu²,
Tanda Li² and Zhongmu Li³

¹*School of Physics and Chemistry, Henan Polytechnic University, Jiaozuo 454000, Henan, China.*

²*Department of Astronomy, Beijing Normal University, Beijing 100875, China.*

³*Institute for Astronomy and History of Science and Technology, Dali University, Dali 671003, China.*

ABSTRACT

We calculated the populations of core-helium-burning (CHeB) stars and found that the secondary red clump (SRC) stars can form an SRC peak in the distributions of the frequency of maximum seismic amplitude (ν_{max}) and mean large-frequency separation ($\Delta\nu$) of CHeB stars when metallicity $Z \geq 0.02$. The ν_{max} and $\Delta\nu$ of CHeB stars are dependent not only on He core mass but on H-shell burning. The SRC peak is composed of the CHeB stars with mass roughly between the critical mass M_{HeF} and $M_{HeF}+0.2$ while He core mass is between about 0.33 and 0.36 M_{\odot} . The location of the SRC peak can be affected by the mixing-length parameter α , metallicity Z , and overshooting parameter δ_{ov} . A decrease in α or increase in Z or δ_{ov} leads to a movement of the SRC peak towards a lower frequency. However, the change in Z and α only slightly affects the value of M_{HeF} but the variation in δ_{ov} can significantly affects the value of M_{HeF} . Thus the SRC peak might aid in determining the value of M_{HeF} and calibrating δ_{ov} . In addition, the effects of convective acceleration of SRC stars and the ν_{max} of ‘semi-degenerate’ stars decreasing with mass result in the appearance of a shoulder between about 40 and 50 μHz in the ν_{max} distribution. However, the convective acceleration of stars with $M < M_{HeF}$ leads to the deficit in the ν_{max} distribution between about 9 and 20 μHz . Moreover, the value of the parameter b of the relation between ν_{max} and $\Delta\nu$ for the populations with $M > M_{HeF}$ is obviously larger than that for the populations with $M < M_{HeF}$.

Key words: stars: evolution; stars: late-type; stars: oscillations.

1 INTRODUCTION

Solar-like oscillations of giant stars were firstly confirmed in a few stars (Frandsen et al. 2002; Barban et al. 2004; De Ridder et al. 2006). And then the presence of radial and non-radial solar-like oscillations in a large sample of red giants was presented by De Ridder et al. (2009). Although only a very limited number of modes ($l \leq 3$) are likely to be observed in solar-like oscillations due to geometrical cancellation effects, the low-degree p-modes of the oscillations can penetrate deep into the interior of stars (Dziembowski & Goode 1997), and each low-degree p-mode carries unique information about the stellar interior. Thus, asteroseismology has the capability to probe the interior of stars and to determine stellar fundamental parameters (Ulrich 1986; Gough 1987; Kjeldsen & Bedding 1995; Christensen-Dalsgaard 2002; Yang & Bi 2007; Yang & Meng 2010; Stello et al. 2009a,b; Kallinger et al. 2010a,b; Mosser et al. 2010).

However, for most of red giants, only the mean large-frequency separation ($\Delta\nu$) and the frequency of maximum seis-

mic amplitude (ν_{max}) have been obtained so far. The oscillation frequencies ν_{max} and $\Delta\nu$ of a large sample of red giants were firstly extracted by Hekker et al. (2009) from the data observed by the first *CO*nvection *RO*tation and *planetary* *Tr*ansits (*CoRoT*) (Baglin et al. 2006) 150-day long run in the direction of the Galactic Centre (LRc01). They found that there is a dominant peak in the distributions of ν_{max} and $\Delta\nu$, respectively, and that there is a tight relation between ν_{max} and $\Delta\nu$, i.e.

$$\Delta\nu \simeq a\nu_{max}^b, \quad (1)$$

where a and b are constant parameters. Using the data observed by *CoRoT* in the opposite direction of LRc01 (LRa01), Mosser et al. (2010) found similar results, except for the locations of the dominant peaks and the values of the parameters a and b . By making use of the data observed by *Kepler* mission (Koch et al. 2010), Huber et al. (2010, 2011) and Hekker et al. (2011b) also obtained very similar results. Moreover, the values of ν_{max} and $\Delta\nu$ of red giants of clusters NGC 6811, NGC 6819, and NGC 6791 have also been extracted by Stello et al. (2010a) and Hekker et al. (2011a). For an ensemble of stars, the ν_{max} and $\Delta\nu$ can be applied to investigate many interesting questions about the Galaxy or

* E-mail: yangwuming@ynao.ac.cn; yang.wuming@yahoo.com.cn

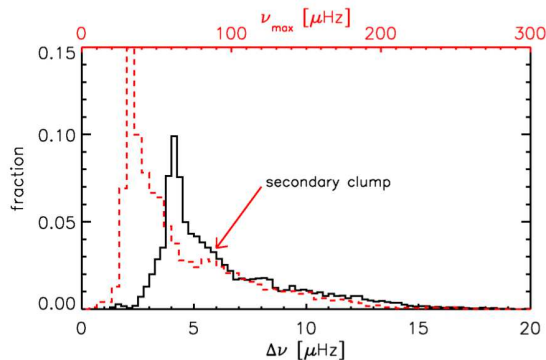


Figure 1. The distribution of ν_{max} (red dashed line and top-axis) and $\Delta\nu$ (black solid line and bottom axis) obtained by Hekker et al. (2011b).

stellar clusters (Miglio et al. 2009, 2012; Miglio 2011; Yang et al. 2010, 2011a; Huber et al. 2010; Mosser et al. 2010; Hekker et al. 2011a,b; Stello et al. 2010a,b, 2011). These studies advanced our understanding of the theory of stellar structure and evolution.

Furthermore, it has been identified that the non-uniform distributions of ν_{max} and $\Delta\nu$ of red giants result from red-clump [core-helium-burning (CHeB)] stars (Miglio et al. 2009; Mosser et al. 2010; Yang et al. 2010; Huber et al. 2010; Hekker et al. 2011b). The dominant peak in the distributions of ν_{max} and $\Delta\nu$, which is located around 30 and 4 μHz for ν_{max} and $\Delta\nu$, respectively, is mainly composed of the stars that are close to the zero-age horizontal branch (ZAHB) (Yang et al. 2010, 2011a). Stars with $\nu_{max} > 40 \mu\text{Hz}$ are mainly red-clump stars with mass larger than $2.0 M_{\odot}$ (Huber et al. 2010). These stars could be attributed to the secondary red clump (SRC) predicted by Girardi (1999) (Miglio et al. 2009; Mosser et al. 2010; Huber et al. 2010; Kallinger et al. 2010b; Hekker et al. 2011b). Moreover, Hekker et al. (2011b) showed that the SRC stars could become a hump in the ν_{max} distribution roughly between 70 and 100 μHz [see Fig. 1 or the Figure 2 in Hekker et al. (2011b)]. Mosser et al. (2010) also showed that the distributions of ν_{max} and $\Delta\nu$ observed by *CoRoT* have a complex structure. The SRC has been identified in the colour-magnitude diagrams of some intermediate-age star clusters, such as NGC 419 in the Small Magellanic Cloud (Girardi et al. 2009) and NGC 1751 in the Large Magellanic Cloud (Rubele et al. 2011). Although the origin of the SRC in clusters is still an open question (Yang et al. 2011b), the SRC should be present in all galactic fields containing stars with an age of about 1 Gyr (Girardi 1999). The SRC is believed to be made of stars whose mass is slightly more massive than the critical mass (M_{HeF}) that is the maximum mass allowing helium flash to occur (Girardi 1999; Yang et al. 2011b).

Stellar models with $M \gtrsim M_{\text{HeF}}$ can be generally evolved from zero-age main sequence (ZAMS) to asymptotic giant branch (AGB) without interruption. However, the models with $M < M_{\text{HeF}}$ are hardly computed through the violent helium flash. Thus, the stars with $M \gtrsim M_{\text{HeF}}$ should be more suitable to study solar-like oscillations of CHeB stars and the effects of convective-core overshooting and other physical processes on the oscillations in details than the stars with $M < M_{\text{HeF}}$. In addition, the asteroseismic detection and study on SRC stars may provide additional constraints on the star-formation history in the Galaxy and allow us to determine the value of M_{HeF} .

In this paper, we mainly focused on the global characteristics of solar-like oscillations of SRC stars and on the effects of convective-core overshooting, mixing-length parameter, and metal-

licity on the characteristics. The paper is organized as follows. We show our stellar models and population-synthesis method in section 2. We present the results in section 3 and discuss and summarize them in section 4.

2 STELLAR MODELS AND POPULATION SYNTHESIS

2.1 Stellar models

We used the stellar evolution code of Eggleton (1971, 1972, 1973) to calculate stellar evolution models. The code has been updated with the recent input physics over the last three decades (Han, Podsiadlowski & Eggleton 1994; Pols et al. 1995, 1998). The equation of state of Eggleton, Faulkner & Flannery (1973) as modified by Pols et al. (1995) and standard mixing-length theory are used in the code. **The value of 2.0 for the mixing-length parameter (α) was calibrated against the Sun.** The convective-core overshooting is treated as the prescription of Schröder, Pols & Eggleton (1997). The value of 0.12 for the overshooting parameter δ_{ov} is chosen to match the properties of ζ Aurigae binaries which span a mass range of 2.5 to $7.0 M_{\odot}$ (Schröder, Pols & Eggleton 1997). The initial hydrogen and helium abundances are assumed to be functions of the metallicity as follows: $X = 0.76 - 3Z$ and $Y = 0.24 + 2Z$. The efficiency of Reimers (1975) mass-loss rate is set to 0.4 for all models. The opacity table for the metallicity is compiled by Chen & Tout (2007) from Iglesias & Rogers (1996) and Alexander & Ferguson (1994). However, element diffusion for helium and metals is not taken into account.

All models with $M \gtrsim M_{\text{HeF}}$ were evolved from ZAMS to AGB stage without interruption. For the low-mass stars ($M < M_{\text{HeF}}$) we were unable to compute through the He-flash. Instead, we constructed ZAHB models using the prescription of Pols et al. (1998). These ZAHB models were evolved up to the AGB stage. It should be noticed that some errors could be introduced in the post He-flash evolution of these constructed ZAHB models (Pols et al. 1998).

In addition, for a star given mass, radius and effective temperature, the theoretical ν_{max} and $\Delta\nu$ were calculated by using scaling equations (Brown et al. 1991; Kjeldsen & Bedding 1995)

$$\nu_{max} = 3050 \frac{M/M_{\odot}}{(R/R_{\odot})^2 \sqrt{T_{eff}/5777K}} \mu\text{Hz}, \quad (2)$$

and

$$\Delta\nu = 134.6 \frac{(M/M_{\odot})^{1/2}}{(R/R_{\odot})^{3/2}} \mu\text{Hz}. \quad (3)$$

Here, the value of 134.6 μHz for $\Delta\nu_{\odot}$ is obtained from the GONG data (Yang & Meng 2009). The accuracy of these estimates is good to within 5% (Stello et al. 2009a).

2.2 Stellar population synthesis

In order to obtain the distributions of ν_{max} and $\Delta\nu$ of SRC stars, we calculated single-star stellar population (SSP). Stellar samples are generated by the Monte Carlo simulation. The basic assumptions for the simulations are as follows. (i) Star formation rate (SFR) is assumed to be a constant. (ii) The age-metallicity relation is taken from Rocha-Pinto et al. (2000) or a constant metallicity is assumed for simplicity. (iii) The lognormal initial mass function (IMF) of Chabrier (2001) is adopted.

Table 1. The values of the critical mass M_{HeF} (in M_{\odot}) estimated from our calculations with $\alpha = 2.0$ and $\delta_{ov} = 0.12$.

Z	0.05	0.04	0.03	0.02	0.01	0.004
M_{HeF}	1.96	1.99	2.01	2.01	1.93	1.83

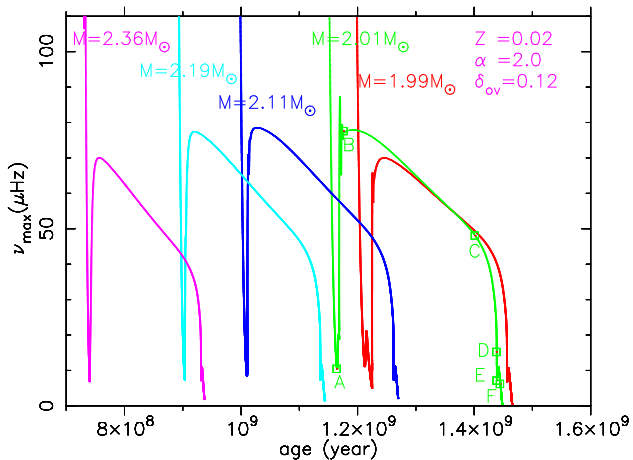


Figure 2. The evolutions of ν_{max} of CHEB stars with different masses. These models were evolved from ZAMS to AGB. For $Z = 0.02$ and $\delta_{ov} = 0.12$, the critical mass M_{HeF} is $2.01 M_{\odot}$. But the minimum mass that can be evolved from ZAMS to AGB without interruption by He-flash is $1.99 M_{\odot}$ in our calculations. Point A corresponds to the FGB tip. Point B indicates the state that the star just reaches the ‘HB’. Point C shows the state that a convective core has formed and central He abundance decreases to about 0.18. Point D represents the state that the central He is completely depleted. Point E shows the state that central temperature and the rate of H-shell burning reaches a maximum, respectively. Point F shows the state that the H-shell is reignited, i.e. the terminal of the early AGB.

3 CALCULATION RESULTS

3.1 The peak of SRC stars

In order to obtain the ν_{max} and $\Delta\nu$ of the populations of SRC stars, we firstly generated a ZAMS sample with mass between 1.80 and $5.0 M_{\odot}$ according to the IMF of Chabrier (2001). Then we computed the evolutions of the models in the sample from high to low mass until calculations were interrupted by a violent He-flash at the tip of first giant branch (FGB). For a given Z , we define M_{HeF} as the mass for which the ν_{max} at the beginning of quiescent helium burning [‘horizontal branch (HB)’]. Hereafter, the ‘HB’ also refers to the similar evolutionary stage of models with $M > M_{\text{HeF}}$ in the Hertzsprung-Russell diagram.] reaches a maximum and He-core mass (M_{HeC}) reaches a minimum. The luminosity of the model with $M = M_{\text{HeF}}$ at the FGB tip almost reaches a minimum. The value of the He-core mass is about $0.33 M_{\odot}$ for $Z = 0.02$ and about $0.34 M_{\odot}$ for $Z = 0.004$. The values of M_{HeF} in Table 1 for different metallicities are estimated from the tracks calculated at an interval less than $0.005 M_{\odot}$. These values are almost not affected by the mixing-length parameter α but can be significantly affected by overshooting parameter δ_{ov} . The stars with mass slightly less than M_{HeF} (for $Z = 0.02$, the mass is between about 1.70 and $2.01 M_{\odot}$) ignite helium under semi-degenerate conditions at core masses between ~ 0.33 and $0.45 M_{\odot}$ (hereafter referred to as *semi-degenerate stars*). However, for the stars with lower mass, helium is ignited in the degenerate core with mass about $0.45 M_{\odot}$ (hereafter referred to as *degenerate stars*) (Pols et al. 1998).

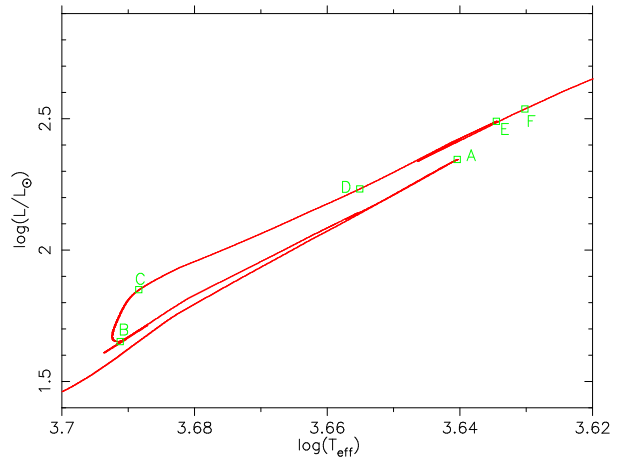


Figure 3. The Hertzsprung-Russell diagram of the model with $M = 2.01 M_{\odot}$ and $Z = 0.02$. The points A, B, C, D, E, and F correspond to the points in Fig. 2.

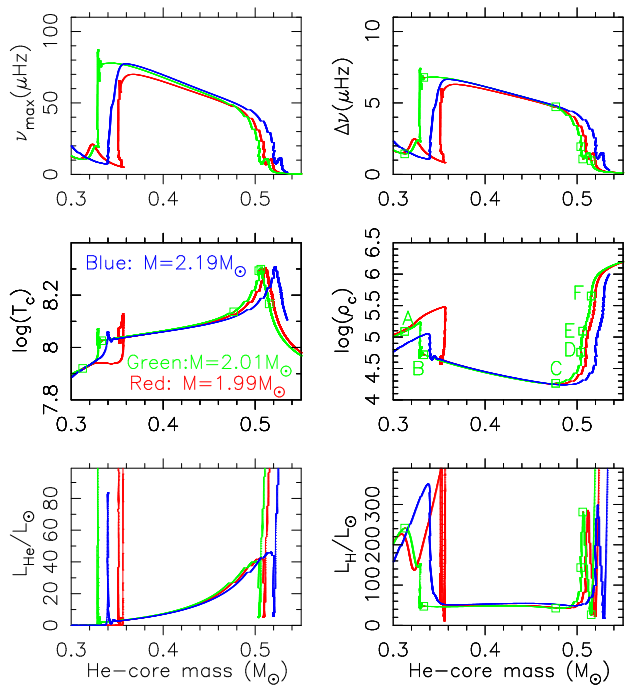


Figure 4. The ν_{max} , $\Delta\nu$, central temperature T_c , central density ρ_c , He-burning luminosity L_{He} , and H-burning luminosity L_{H} as a function of He-core mass.

The evolutions of ν_{max} of CHEB stars with the same Z , α , and δ_{ov} but different masses are shown in Fig. 2. The ν_{max} , $\Delta\nu$, central temperature T_c , central density ρ_c , He-burning luminosity L_{He} , and H-burning luminosity L_{H} of three models are shown in Fig. 4 as a function of He-core mass. Several specifically evolutionary states are marked in the Figs. 2, 3 and 4. The point A on the track of $M = 2.01 M_{\odot}$ corresponds to the FGB tip in the Hertzsprung-Russell diagram (see Fig. 3), while the point B represents the beginning of the ‘HB’. From point B to C, helium burning proceeds quietly in the He core, the central He abundance Y_c decreases gradually to about 0.18, and a convective core has formed in the stars. Then owing to mixing in the core, there is a sudden depletion of He fuel over a large region, which leads to a rapid contraction of the core, increase in central temperature and expan-

sion of the radius of the star on a thermal time-scale. This results in that the star evolves quickly from $Y_c \approx 0.18$ to $Y_c \approx 0$ (point D) and that the ν_{max} decreases rapidly. We labeled this evolutionary phase as ‘convective acceleration’. From point D, the star evolves through the early AGB. As the He abundance in central regions goes to zero, the He-exhausted core contracts and heats up while the H-rich envelope expands and cools. Cooling in the H-rich envelope is so effective that the H-shell burning begins to extinguish (Chiosi et al. 1992) and the envelope recontracts (point E), which leads to the increase in ν_{max} and $\Delta\nu$. Eventually the contraction is prevented by the efficient He-shell burning. Then the stars begin to expand and their ν_{max} and $\Delta\nu$ begin to decrease. The H shell is reignited at point F. From then on H-shell burning dominates energy production. Thus there is a hook between point E and F of the evolutionary track of ν_{max} , and the stars take a long time from E to F. As a consequence, there might be a peak (AGB peak) in the ν_{max} distribution around 10 μHz .

When stars arrive at the ‘HB’, their ν_{max} and $\Delta\nu$ are mainly dependent on their He-core mass and H-shell burning. When the He-core mass is larger than about $0.36 M_\odot$, the ν_{max} and $\Delta\nu$ obviously decrease with the increase in He-core mass. For the semi-degenerate stars, when they reach the ‘HB’, their He-core masses increase fast with decreasing initial mass. Thus the values of ν_{max} and $\Delta\nu$ of these stars decrease rapidly with decreasing mass. For example, when the mass decreases from 2.01 to $1.99 M_\odot$, the He-core mass increases from about 0.33 to $0.37 M_\odot$ and the value of ν_{max} decreases from about 78 to 70 μHz (see Fig. 2). Moreover, for a given mass star, when the energy production of H-shell burning arrives at a minimum, its ν_{max} almost reaches a maximum. When the He-core mass of the model with $M = 2.01 M_\odot$ increases from about 0.33 to $0.36 M_\odot$, the energy production of CHeB increases from about 2.0 to $3.6 L_\odot$, but the energy from H-shell burning decreases from about 47.5 to $46.4 L_\odot$ and reaches a minimum. The total energy production is almost constant. The changes in the luminosity, radius, and mean density of this model are insignificant in this stage. As a consequence, its ν_{max} and $\Delta\nu$ are almost unchanged. For the star with $M = 2.19 M_\odot$, when it reaches the ‘HB’, its He-core mass is about $0.36 M_\odot$, and its energy production of H-shell burning reaches a minimum. Its ν_{max} reaches a maximum at this time and is almost equal to that of model with $M = 2.01 M_\odot$ at $M_{\text{HeC}} \simeq 0.36 M_\odot$ (see Fig. 4). When the stars with mass between 2.01 and $2.19 M_\odot$ arrive at the ‘HB’, their He-core masses are between about 0.33 and $0.36 M_\odot$. Their energy productions of H-shell burning also reach a minimum as their $M_{\text{HeC}} \simeq 0.36 M_\odot$. The ν_{max} of these models is similar to that of model with $M = 2.01 M_\odot$. For the stars with $M > 2.19 M_\odot$, when they arrive at the ‘HB’, their He-core masses are larger than $0.36 M_\odot$. The more massive the star, the larger the He-core mass, thus the smaller the ν_{max} and $\Delta\nu$. For example, when the mass increases from 2.19 to $2.36 M_\odot$, the value of ν_{max} decreases from 77.5 to 70.0 μHz (see Fig. 2).

Figure 5 shows the distributions of ν_{max} and $\Delta\nu$ of the CHeB populations with mass between 5.0 and $1.99 M_\odot$ and $Z = 0.02$ as a function of stellar age and the histograms of the ν_{max} and $\Delta\nu$. The convective acceleration leads to the absence of the SRC stars with $\nu_{max} < 50 \mu\text{Hz}$ in the ν_{max} distribution. The CHeB stars with mass between about 2.19 and $2.01 M_\odot$ form an SRC peak at about $75\text{--}78 \mu\text{Hz}$ for ν_{max} and at about $6.5\text{--}6.8 \mu\text{Hz}$ for $\Delta\nu$. If the stars with mass less than $1.99 M_\odot$ were included, the peak at about $50 \mu\text{Hz}$ for ν_{max} and about $5 \mu\text{Hz}$ for $\Delta\nu$ might disappear, which depends on the properties of semi-degenerate stars. However, the SRC peak can not be affected by the stars because the ν_{max} and $\Delta\nu$ of

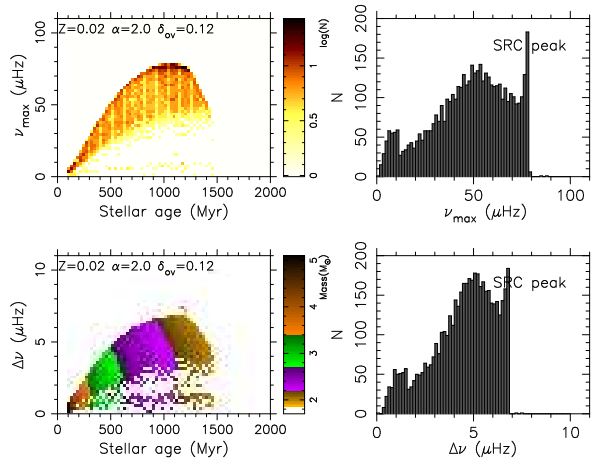


Figure 5. The distributions of ν_{max} and $\Delta\nu$ of the CHeB stars with $M \gtrsim M_{\text{HeF}}$ as a function of stellar age and the histograms of the ν_{max} and $\Delta\nu$ of these stars.

semi-degenerate stars decrease rapidly with decreasing mass (see the comparison in Fig. 10). Moreover, the peak located at about 10 μHz for ν_{max} and 1 μHz for $\Delta\nu$ is mainly composed of the CHeB stars with $M \gtrsim 4.0 M_\odot$ and the stars with lower mass but undergone convective acceleration. The stars with mass between about 2.19 and $2.01 M_\odot$ have an almost equal ν_{max} when they arrive at the ‘HB’. However, for the stars with $M > 2.19$ ($M < 2.01$) M_\odot , the value of ν_{max} increases (decreases) with decreasing mass. This might provide us an opportunity to distinguish the SRC stars from others in the asteroseismical observations of a large sample of stars.

3.2 The effect of metallicity on the distributions of ν_{max} and $\Delta\nu$ of SRC stars

We calculated the CHeB populations with the same α and δ_{ov} but different metallicities. The distributions of ν_{max} and $\Delta\nu$ of the populations are shown in Figs. 6 and 7. Our calculations show that the SRC peak is present in the histograms of ν_{max} and $\Delta\nu$ of populations with $Z \gtrsim 0.02$. However, when the metallicity increases from 0.02 to 0.05, the value of M_{HeF} decreases from 2.01 to $1.96 M_\odot$ and the location of the SRC peak moves from about 78 to 58 μHz for ν_{max} . When the stars with $M = M_{\text{HeF}}$ and $Z \gtrsim 0.02$ arrive at the ‘HB’, they have almost the same He core, but their radii and the energy production of H-shell burning increase with increasing metallicity, i.e. the higher the metallicity the greater the energy production of H-shell burning and the less the contraction of H-rich envelope when the stars evolve from the tip of the FGB to the ‘HB’. Thus, the mean density of critical mass models decreases with increasing metallicity. Hence the values of the ν_{max} and $\Delta\nu$ of the models decrease with increasing metallicity. Therefore, the frequency of the location of the SRC peak decreases with increasing metallicity.

However, the SRC peak does not appear in the histograms of ν_{max} and $\Delta\nu$ of the populations with $Z = 0.01$ and 0.004. Figure 8 shows the evolutions of ν_{max} of CHeB stars with the same metallicity (0.004) but different masses. The maximum of ν_{max} of the CHeB stars with $M > M_{\text{HeF}}$ ($1.83 M_\odot$) decreases with increasing stellar mass, which is different from the result of populations with $Z = 0.02$. The He-core mass of the model with $M = 1.83 M_\odot$ and $Z = 0.004$ is about $0.34 M_\odot$ when the star arrive at the ‘HB’, the energy production of H-shell burning reaches a minimum at the

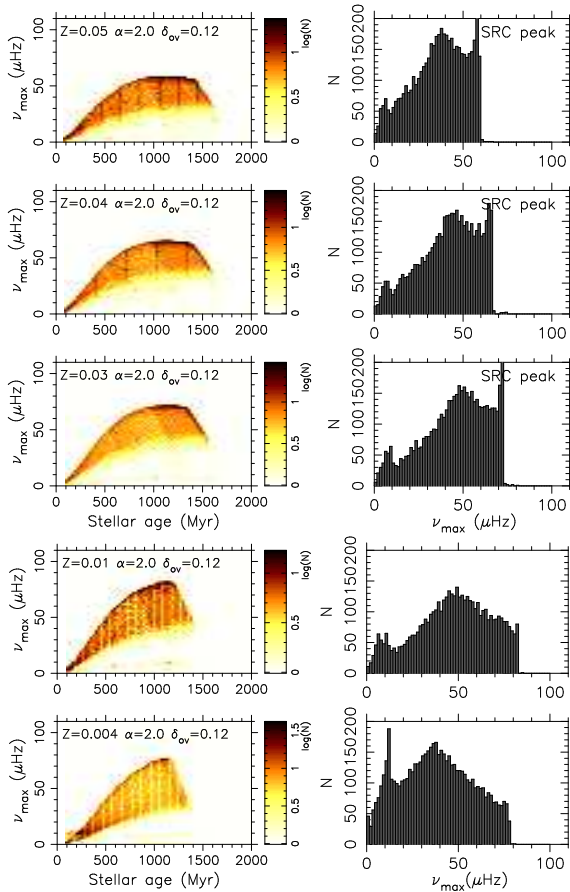


Figure 6. Same as Fig. 5 but for different metallicities.

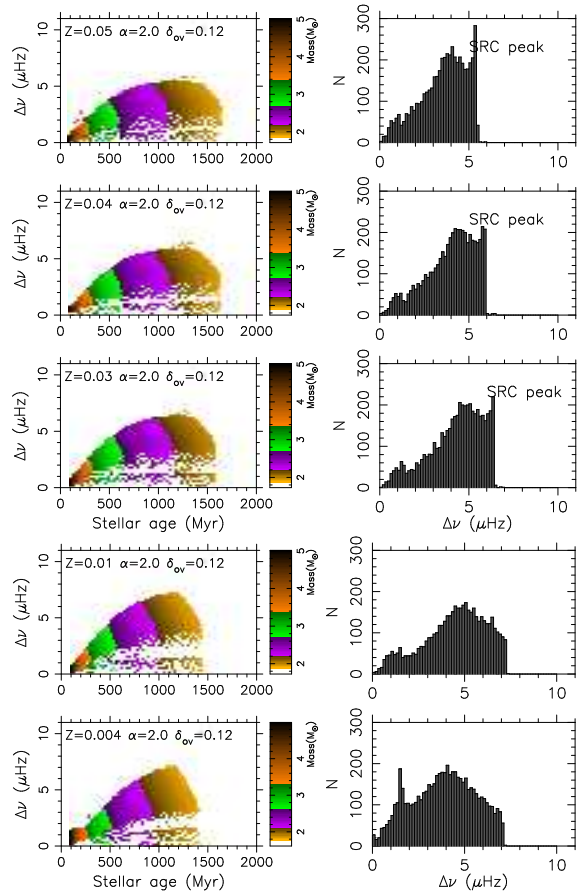


Figure 7. Same as Fig. 5 but for different metallicities.

same time (see Fig. 9). The burning rates of central helium and H-shell increase with the increase in the He-core mass, which makes the star to expand. Thus its ν_{max} and $\Delta\nu$ decrease with the increase in the He-core mass. When a star with $M > 1.83 M_{\odot}$ arrives at the ‘HB’, its He-core mass is larger than $0.34 M_{\odot}$, its energy production of H-shell burning reaches a minimum at the same time, and its ν_{max} arrives at a maximum. The more massive the stellar mass the bigger the He-core mass, the smaller the ν_{max} . Thus the SRC peak can not be formed in the histogram of ν_{max} of populations with $Z = 0.004$. The characteristics of ν_{max} and $\Delta\nu$ of populations with $Z = 0.01$ are similar to those of populations with $Z = 0.004$.

3.3 The effects of the mixing-length parameter, degenerate and semi-degenerate stars on the SRC peak

When $\alpha = 2.0$ and $\delta_{ov} = 0.12$, the ages of the stars with mass slightly larger than M_{HeF} are located roughly between 1.0 and 1.3 Gyr as the stars reach the ‘HB’. According to the age-metallicity relation of Rocha-Pinto et al. (2000), the metallicity of the stars with an age of about 1.2 Gyr is around 0.04. For the populations with $Z = 0.04$, $\alpha = 2.0$, and $\delta_{ov} = 0.12$, the SRC peak is located at about 63-67 μHz in the ν_{max} distribution and at around 5.7-6.0 μHz in the $\Delta\nu$ distribution. We note that, in the figures 4 and 5 of Mosser et al. (2010), there seems to be a bump at around 65 μHz in the ν_{max} distribution and at about 5.5-6.0 μHz in the $\Delta\nu$ distribution, which may be corresponding to our SRC peak. However, the secondary clump found by Hekker et al. (2011b) in the ν_{max} dis-

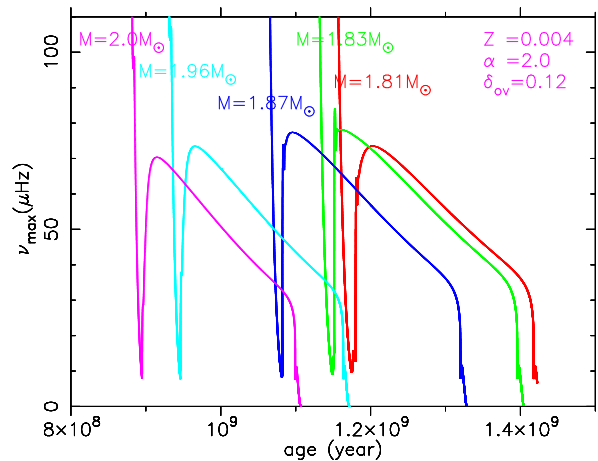


Figure 8. Same as Fig. 2 but for $Z = 0.004$. For $Z = 0.004$ and $\delta_{ov} = 0.12$, the critical mass M_{HeF} is $1.83 M_{\odot}$.

tribution is located roughly between 70 and 100 μHz . Increasing α can decrease stellar radius, i.e. can increase ν_{max} and $\Delta\nu$. Thus we calculated the populations with a bigger α .

Figure 10 shows the distributions of ν_{max} and $\Delta\nu$ of the CHeB populations with $Z = 0.04$, $\delta_{ov} = 0.12$, and $\alpha = 2.7$. The value of M_{HeF} is about $1.98 M_{\odot}$ for this set of parameters. The change in α hardly affects the value of M_{HeF} . However the location of SRC peak moves from about 65 to 80 μHz for ν_{max} and from 5.8 to 7.0 μHz for $\Delta\nu$ when the value of α increases from 2.0

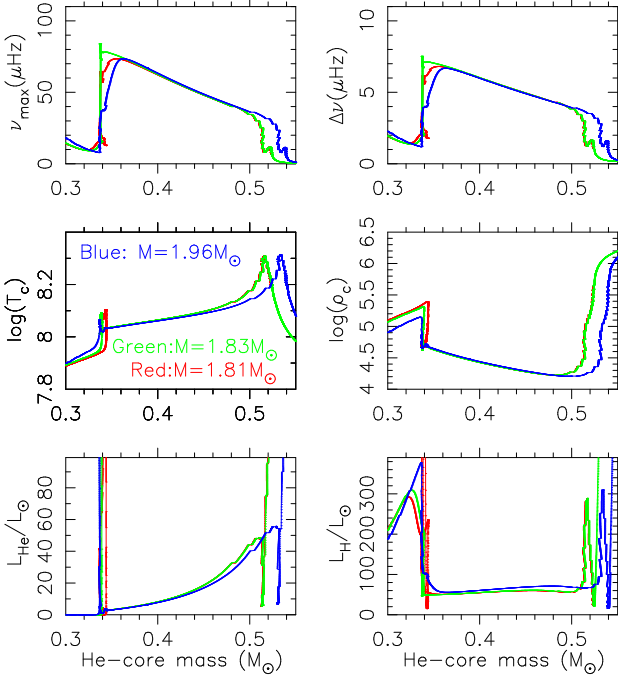


Figure 9. Same as Fig. 4 but for $Z = 0.004$. For $Z = 0.004$ and $\delta_{ov} = 0.12$, the critical mass M_{HeF} is $1.83 M_{\odot}$.

to 2.7. Red giant stars have a deep convective envelope. Increasing α leads to an increase in the efficiency of convective energy transport, which can cause the more contraction of the convective envelope. The larger the α the more the contraction. However, the change in α barely affects the nuclear reaction in stellar interior. Therefore the variation of the mixing-length parameter has almost no influence on the age and luminosity but can change the mean density of models. Hence, the values of ν_{max} and $\Delta\nu$ increase with increasing α .

In order to investigate the effect of stars with $M < M_{\text{HeF}}$ on the SRC peak, the panels B's and D's of Fig. 10 show the distributions of ν_{max} and $\Delta\nu$ of populations with $M > 1.48 M_{\odot}$. These panels show that the SRC peak can not be affected by the degenerate and semi-degenerate stars. The dominant peak of ν_{max} and $\Delta\nu$ of these populations is located at about 33 and 4 μHz , respectively, and is mainly caused by the stars with age larger than about 2.0 Gyr. The value of ν_{max} and $\Delta\nu$ of the CHeB stars with $M < 1.48 M_{\odot}$ is almost less than 40 and 4 μHz , respectively. These stars can not affect the distributions of ν_{max} larger than 40 μHz and $\Delta\nu$ larger than 4.0 μHz unless their mass-loss rate is very high in red giant stage (Yang et al. 2010), but can slightly affect the location of the dominant peak.

Moreover, panel B2 of Fig. 10 shows that there is a shoulder in the ν_{max} histogram roughly between 40 and 50 μHz . The convective acceleration of stars with $M \gtrsim M_{\text{HeF}}$ leads to the absence of stars with ν_{max} less than about 50 μHz and age between about 0.9 and 1.5 Gyr in the panels A1 and B1 of Fig. 10. The panel A2 of Fig. 10 shows that the number of stars with $M \gtrsim M_{\text{HeF}}$ increase when ν_{max} decreases from 70 to about 50 μHz , and then decrease with the decrease in ν_{max} . We marked this peak in the ν_{max} histogram around 50 μHz as convective acceleration peak. The value of about 50 μHz is determined by the convective acceleration of stars with $M \gtrsim M_{\text{HeF}}$. However, the value of ν_{max} of semi-degenerate stars decreases with decreasing stellar mass. In addition, according to the IMF, the lower the stellar mass the greater

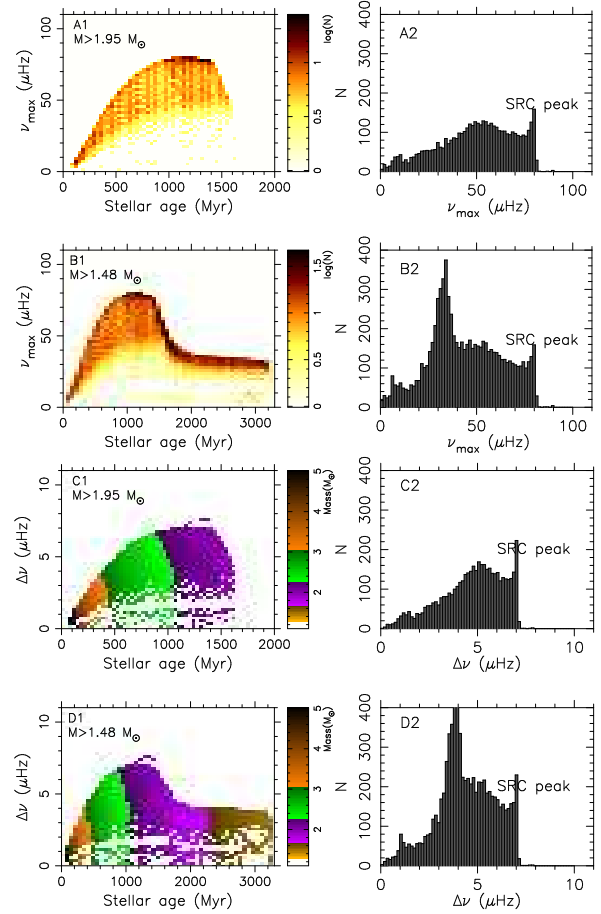


Figure 10. Same as Fig. 5 but for the populations with $Z = 0.04$, $\delta_{ov} = 0.12$, and $\alpha = 2.7$. The value of M_{HeF} for $Z = 0.04$, $\delta_{ov} = 0.12$, and $\alpha = 2.7$ is $1.98 M_{\odot}$. The populations with $M > 1.48 M_{\odot}$ include the degenerate and semi-degenerate stars.

the number of stars. Thus the number of stars with $M < M_{\text{HeF}}$ increase with the decrease in ν_{max} . The shoulder derives from that the decrease in the number of stars with $M > M_{\text{HeF}}$ is just counteracted by the increase in the number of stars with $M < M_{\text{HeF}}$ between about 40 and 50 μHz .

3.4 The effects of convective core overshooting on the SRC peaks

Figs.11 and 12 show the distributions of ν_{max} and $\Delta\nu$ of populations with the same Z and α but different δ_{ov} . For the populations with $Z = 0.04$ and $\alpha = 2.7$, when the value of the δ_{ov} decreases from 0.15 to 0.0, the value of M_{HeF} increases from 1.89 to $2.24 M_{\odot}$ and the location of the SRC peak moves from about 76 to 91 μHz for ν_{max} and from about 6.7 to 7.6 μHz for $\Delta\nu$. Moreover, the age of the stars composed the SRC peak is between about 0.6 and 0.8 Gyr for $\delta_{ov} = 0.0$ but the age is between around 1.2 and 1.6 Gyr for $\delta_{ov} = 0.15$. This is mainly caused by the change in M_{HeF} . We listed the values of the M_{HeF} for different δ_{ov} in Table 2 and plotted the evolutionary tracks of the models with the critical mass in Fig. 13. An increase in δ_{ov} prolongs the lifetime of core H burning by feeding more H-rich material into the core, which can enhance the He core mass left behind and strongly change the global characteristics of the following giant stages (Schróder, Pols & Eggleton 1997). Thus the value of M_{HeF} decreases with increasing δ_{ov} .

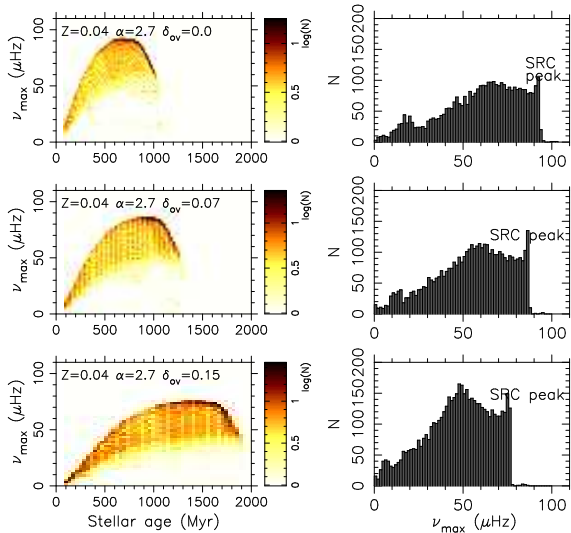


Figure 11. Same as Fig. 10 but for the populations with different δ_{ov} .

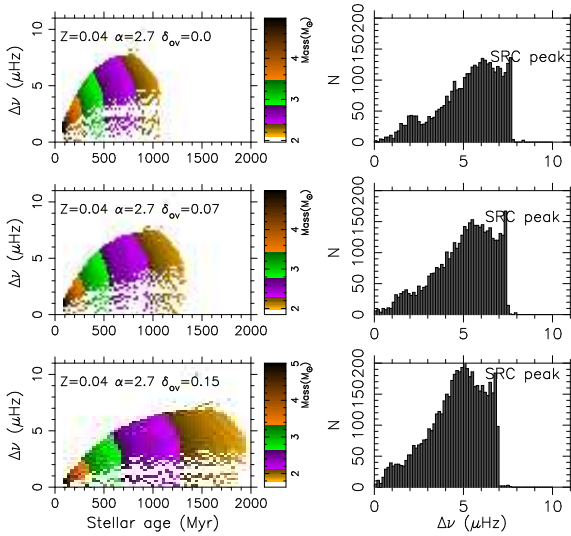


Figure 12. Same as Fig. 10 but for the populations with different δ_{ov} .

When the models with these critical masses reach the ‘HB’, they have almost the same He-core mass, central temperature, central density, central pressure, and nuclear energy production. However, the larger the critical mass the smaller the stellar radius, and the more the contraction of H-rich envelope when the stars evolve from the FGB tip into the ‘HB’, i.e. the higher the mean density. Thus the decrease in δ_{ov} leads to a movement of the location of SRC peak towards a higher frequency. However, the change in δ_{ov} has almost no influence on the effective temperature of SRC stars (see Fig. 13).

Table 2. The values of the critical mass M_{HeF} (in M_{\odot}) estimated from our calculations with $\alpha = 2.7$ and $Z = 0.04$.

δ_{ov}	0.15	0.12	0.10	0.07	0.00
M_{HeF}	1.89	1.98	2.03	2.11	2.24

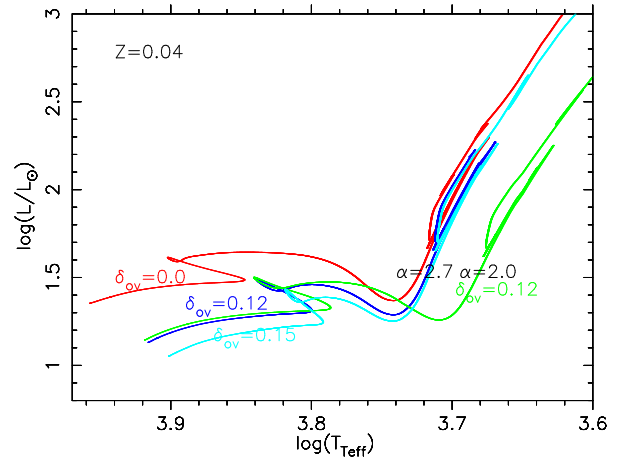


Figure 13. The evolutionary tracks of the models with $M = M_{\text{HeF}}$. These models have the same metallicity ($Z = 0.04$) but different α and δ_{ov} which are labeled on their tracks.

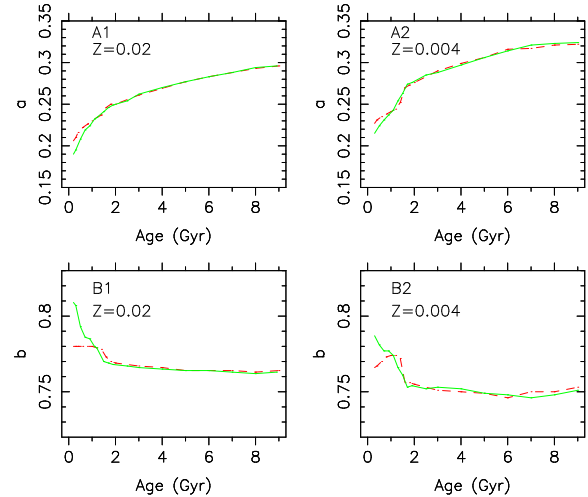


Figure 14. The changes of parameters a and b with the age of populations. The dashed lines show the results of the SSP without spread in age, while the solid lines indicate those of the SSP with a spread in age of 200 Myr.

3.5 Parameters a and b

Figure 14 shows the parameters a and b as a function of population age. For the populations with $Z = 0.02$, the value of a increases from about 0.2 to 0.3 when the age of populations increases from about 0.2 to 9.0 Gyr. However, the value of parameter b is about 0.78 and almost unchanged when age < 1.2 Gyr and is around 0.764 but slightly decreases with age when age > 2.0 Gyr. When $1.2 \text{ Gyr} < \text{age} < 2.0 \text{ Gyr}$, the value of b decreases with age. Recent observations show that the intermediate-age star clusters may be composed of stars with a non-uniform age [a spread in age of about 200–300 Myr (Mackey & Broby Nielsen 2007; Milone et al. 2009)]. Our calculations show that a spread in age of 200 Myr can significantly affect the parameters a and b of the populations with age less than about 2 Gyr but hardly affects those of the populations with age > 2 Gyr. The spread leads to an increase in b but a decrease in a for the populations with age less than about 1.2 Gyr and a decrease in b for the populations with age between about 1.2 and 2.0 Gyr. For the populations with the spread in age, the value of b decreases fast from about 0.81 to 0.77 when the age of the pop-

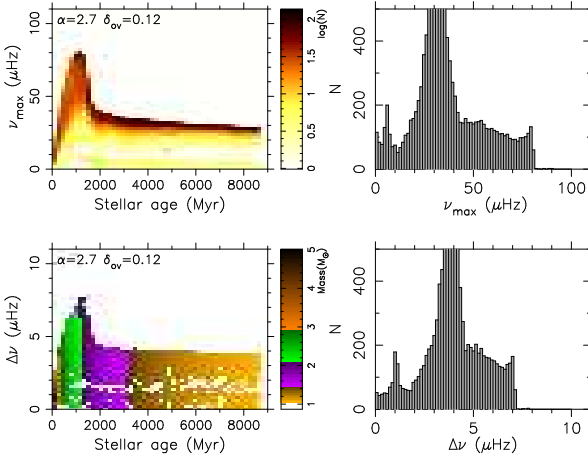


Figure 15. Same as Fig. 4 but for the populations with age between 0 and 9 Gyr.

ulations increases from 0.2 to 2.0 Gyr. Moreover, our calculations show that the characteristics of a and b of populations with $Z = 0.03, 0.04$ and 0.05 are almost the same as those of populations with $Z = 0.02$. However, the value of a of populations with $Z = 0.004$ is larger than that of populations with $Z = 0.02$. But the value of b of populations with $Z = 0.004$ is smaller than that of populations with $Z = 0.02$. When the age of populations is larger than about 2 Gyr, the value of b for the populations with $0.02 \leq Z \leq 0.04$ is located between about 0.77 and 0.76; however, that for populations with $Z = 0.004$ is located between about 0.76 and 0.75. The value of b of populations with $Z = 0.01$ is located between that of populations with $Z = 0.02$ and populations with $Z = 0.004$. Furthermore, our calculations show that a change in the mixing-length parameter does not significantly affect the parameters a and b . However, the decrease in δ_{ov} can lead to a small increase in b and decrease in a for the populations with $M \gtrsim M_{\text{HeF}}$.

The value of parameters a and b is about 0.20 and 0.79 for NGC 6811 (~ 1.0 Gyr), 0.24 and 0.77 for NGC 6819 (~ 2.5 Gyr), and 0.28 and 0.75 for NGC 6791 (~ 8.5 Gyr), respectively (Hekker et al. 2011a). The characteristics of the a and b of populations with the spread in age of 200 Myr are more consistent with these obtained by Hekker et al. (2011a) than those of populations with a uniform age.

3.6 A synthesis result

We computed the stellar populations with $\alpha = 2.7$, $\delta_{ov} = 0.12$, and $Z = 0.004, 0.01, 0.02, 0.03, 0.04$ and 0.05 . However, the metallicity of the populations in the Galaxy is believed to change with age. We estimated the metallicity from the age-metallicity relation of Rocha-Pinto et al. (2000). By interpolating, we obtained the CHeB populations with age between 0 and 9 Gyr and metallicity changing with age. The distributions of ν_{max} and $\Delta\nu$ of the populations are shown in Fig. 15. The dominant peak is located about 30 and 3.9 μHz in the ν_{max} and $\Delta\nu$ distribution, respectively. The SRC peak is situated at around 78 and 7 μHz in the ν_{max} and $\Delta\nu$ distribution, respectively. The shoulder is located between about 43 and 54 μHz in the ν_{max} distribution. However, there is not a significant shoulder in the $\Delta\nu$ distribution. Moreover, there is a deficit in the ν_{max} distribution between about 9 and 20 μHz and in the $\Delta\nu$ distribution between around 1.2 and 2.5 μHz , which is caused by the convective acceleration of CHeB stars. The peak in the ν_{max} histogram about

7 μHz and in the $\Delta\nu$ histogram around 1 μHz is mainly composed of the CHeB stars with $M \gtrsim 4.0 M_{\odot}$ and the early AGB stars. This peak exists in the distributions of ν_{max} and $\Delta\nu$ observed by the *CoRoT* (Mosser et al. 2010; Huber et al. 2010). The deficit in the ν_{max} histogram between about 10 and 20 μHz and in the $\Delta\nu$ histogram between around 1.5 and 2.5 μHz observed by *CoRoT* (Mosser et al. 2010) might be partly caused by the convective acceleration.

4 DISCUSSIONS AND CONCLUSIONS

The value of M_{HeF} obtained from our definition is slightly different from that obtained from the definition of Pols et al. (1998) who defines M_{HeF} as the mass for which the luminosity at the FGB tip reaches a minimum and the core mass at He ignition is about $0.33 M_{\odot}$. According to Pols et al. (1998) definition, we obtained the value of M_{HeF} is $1.994 M_{\odot}$ for $Z = 0.02$, $\alpha = 2.0$, and $\delta_{ov} = 0.12$. The value is consistent with that obtained by Pols et al. (1998). Our calculations show that the maximum of ν_{max} of the model with $M = 1.994 M_{\odot}$ is about 76 μHz on the ‘HB’, which is less than the value of 78 μHz of the model with $M = 2.01 M_{\odot}$.

The SRC peak can appear in the distributions of ν_{max} and $\Delta\nu$ of populations with $Z \geq 0.02$ in our simulations. The location of the SRC peak can be affected by the parameters Z , α , and δ_{ov} . An increase in α or decrease in Z or δ_{ov} can lead to an increase in the frequency of the location of the SRC peak. The change in Z or α can significantly affect the effective temperature of the populations of SRC stars rather than the age of the populations and the value of M_{HeF} for $Z \geq 0.02$. However, the variation in δ_{ov} can significantly affect the value of M_{HeF} and the age of the populations rather than the effective temperature. According to the formulas (2) and (3), the mass of a star can be estimated from its ν_{max} , $\Delta\nu$ and effective temperature T_{eff} . If the frequency of the location of the SRC peak can be obtained from observations, which may aid in determining the value of M_{HeF} and calibrating the overshooting parameter δ_{ov} . Moreover, The SRC peak is mainly composed of CHeB stars with mass between about M_{HeF} and $M_{\text{HeF}} + 0.2$ whose He-core masses are between about 0.33 and $0.36 M_{\odot}$. Because the mass range of the SRC peak stars is very limited, the SRC peak in the histograms of the ν_{max} and $\Delta\nu$ may aid in determining the star-formation rate in the Galaxy or star clusters.

The SRC peak is considerable in our simulations. Comparing with the dominant peak, it is, however, insignificant. If the observed SRC stars have different Z , α and δ_{ov} , the SRC peak might become incon siderable.

The appearance of the shoulder in the histogram of ν_{max} is related to the convective acceleration of stars with mass $\gtrsim M_{\text{HeF}}$ and the ν_{max} of semi-degenerate stars decreasing with mass. The degenerate and semi-degenerate zero-age models are always constructed from a non-degenerate model by mass loss. The ν_{max} and $\Delta\nu$ of these models are mainly dependent on the He-core mass of the zero-age models rather than other parameters. We do not know the exact value of the He-core mass of stars with $M < M_{\text{HeF}}$ when they reach the ‘HB’. A small change in the He-core mass can lead to an obvious variation in the ν_{max} of semi-degenerate stars. Thus the distributions of ν_{max} and $\Delta\nu$ of semi-degenerate stars may be affected by the construction method of the ZAHB models. If the ν_{max} of semi-degenerate stars decreases with mass too fast, the increase in the number of semi-degenerate stars with decreasing ν_{max} can not counteract the decrease in the number of stars with $M > M_{\text{HeF}}$ between about 40 and 50 μHz , the convective ac-

celeration peak will appear in the simulated histogram of ν_{max} of populations including semi-degenerate and degenerate stars, while the upper boundary of the shoulder location will move to a lower frequency, i.e. the shoulder might be replaced by a narrower shoulder plus a convective acceleration peak. The frequency of the upper boundary of the shoulder or the location of convective acceleration peak is mainly determined by the frequency where the convective acceleration of SRC stars begins. The value of this frequency can be affected by the parameters Z , α and δ_{ov} . For example, for populations with $Z = 0.04$, the value is around $54 \mu\text{Hz}$ for $\alpha = 2.7$ but is about $47 \mu\text{Hz}$ for $\alpha = 2.0$. However, the frequency of the lower boundary of the shoulder is mainly determined by the degenerate stars. The effect of Z , α and δ_{ov} on the lower boundary is harder to study by evolving stellar models than that on the upper boundary. A detailed statistical study on the red giant stars with observed $\nu_{max} > 40 \mu\text{Hz}$ would provide additional constraints on the theory of structure and evolution of semi-degenerate and SRC stars.

The SRC and semi-degenerate stars with the same ν_{max} have different $\Delta\nu$, i.e. the values of parameters a and b for SRC stars are different from those for semi-degenerate stars, which leads to a small difference between the ν_{max} and $\Delta\nu$ distributions. For example, the shoulder is less significant in the $\Delta\nu$ distribution than that in the ν_{max} distribution.

The parameter a of CHEB populations increases with the age of populations in the range of about $0.20 - 0.33$. The value of the parameter b for populations with $M > M_{\text{HeF}}$ (age $\lesssim 1.1$ Gyr) is obviously larger than that for the populations with $M < M_{\text{HeF}}$. The value of b for old populations is approximately equal. In general, a spread in the age of populations leads to a decrease in a and increase in b for the populations with $M \gtrsim M_{\text{HeF}}$ but results in a small increase in a and decrease in b for the populations with $M < M_{\text{HeF}}$.

When the star with $M = M_{\text{HeF}}$ and $Z = 0.02$ evolved into the ‘HB’, its He-core mass is about $0.33 M_{\odot}$. When the He-core mass increases from about 0.33 to $0.36 M_{\odot}$, the energy production of He burning increases slightly but that of H-shell burning decreases and reaches a minimum, the total energy production is almost constant. The ν_{max} and $\Delta\nu$ of this model is almost unchanged in this phase. When the stars with mass slightly larger than M_{HeF} (roughly between M_{HeF} and $M_{\text{HeF}} + 0.2$) and $Z = 0.02$ arrive at the ‘HB’, their He-core masses are between 0.33 and $0.36 M_{\odot}$ and their ν_{max} and $\Delta\nu$ are almost equal. Our simulations show that these stars can form an SRC peak in the histograms of ν_{max} and $\Delta\nu$ of the CHEB populations. The SRC peak can also appear in the histograms of ν_{max} and $\Delta\nu$ of the CHEB populations with $Z = 0.03, 0.04$, and 0.05 . However, it does not exist in the histograms of ν_{max} and $\Delta\nu$ of the CHEB populations with $Z = 0.01$ and 0.004 . The SRC peak is present in the histograms of ν_{max} and $\Delta\nu$ of the CHEB populations calculated according to the age-metallicity relation of Rocha-Pinto et al. (2000) too. The SRC peak location can be affected by the mixing-length parameter α , core overshooting parameter δ_{ov} and metallicity Z . An increase in α or decrease in δ_{ov} or Z leads to a movement of the peak location towards a higher frequency. The change in δ_{ov} can significantly affect the value of M_{HeF} but hardly affects the effective temperature of the CHEB populations, which is different from the effects of α and Z . The SRC peak would aid in determining the value of M_{HeF} and calibrating the overshooting parameter δ_{ov} . Moreover, the convective acceleration in the stars with $M \gtrsim M_{\text{HeF}}$ and the ν_{max} of semi-degenerate stars decreasing with mass result in the appearance of a shoulder in the ν_{max} distribution. The convective acceleration of stars with $M < M_{\text{HeF}}$ leads to the deficit in the

ν_{max} histogram between about 9 and $20 \mu\text{Hz}$ and in the $\Delta\nu$ histogram between about 1.5 and $2.5 \mu\text{Hz}$.

ACKNOWLEDGMENTS

This work was supported by China Postdoctoral Science Foundation funded project 20100480222, the Ministry of Science and Technology of the People’s republic of China through grant 2007CB815406, the NSFC through grants 10773003, 10933002, 11003003, 10963001, and the Project of Science and Technology from the Ministry of Education (211102) .

REFERENCES

- Alexander D. R., Ferguson J. W., 1994, ApJ, 437, 879
 Baglin A. et al., 2006, in ESA Special Publication, Vol. 1306, ESA Special Publication, ed. M. Fridlund, A. Baglin, J. Lochard and L. Conroy, p.33
 Barban C. et al., 2004, in Danesy D., ed., ESA SP-559, Proc. SOHO 14/GONG 2004 Workshop, Helio- and Asteroseismology: Towards a Golden Future. ESA Publ., Noordwijk, p. 113
 Brown T. M., Gilliland R. L., Noyes R. W., Ramsey L. W., 1991, ApJ, 368, 599
 Chabrier G., 2001, ApJ, 554, 1274
 Chen X., Tout C.A., 2007, ChJAA, 7, 245
 Chiosi C., Bertelli G., Bressan A., 1992, ARA&A, 30, 235
 Christensen-Dalsgaard J., 2002, Reviews of Modern Physics, 74, 1073
 De Ridder J., Barban C., Carrier F., Mazumdar A., Eggenberger P., Aerts C., Deruyter S., Vanautgaerden J., 2006, A&A, 448, 689
 De Ridder J. et al., 2009, Nature, 459, 398
 Dziembowski W. A., Goode, P., 1997, A&A, 317, 919
 Eggleton P. P., 1971, MNRAS, 151, 351
 Eggleton P. P., 1972, MNRAS, 156, 361
 Eggleton P. P., 1973, MNRAS, 163, 279
 Eggleton P. P., Faulkner J., Flannery B. P., 1973, A&A, 23, 325
 Frandsen S. et al., 2002, A&A, 394, L5
 Frandsen S. et al., 2007, A&A, 475, 991
 Girardi L., 1999, MNRAS, 308, 818
 Girardi L., Rubele S., Kerber L., 2009, MNRAS, 394, L74
 Gough D. O., 1987, Nature, 326, 257
 Han Z., Podsiadlowski P., Eggleton P. P., 1994, MNRAS, 270, 121
 Hekker S. et al., 2009, A&A, 506, 465
 Hekker S. et al., 2011a, A&A, 530A, 100
 Hekker S. et al., 2011b, MNRAS, 414, 2594
 Huber D. et al., 2010, ApJ, 723, 1607
 Huber D. et al., 2011, ApJ, 743, 143
 Iglesias C. A., Rogers F. J., 1996, ApJ, 464, 943
 Kallinger T. et al., 2010a, A&A, 509, A77
 Kallinger T. et al., 2010b, A&A, 522, A1
 Kjeldsen H., Bedding T. R., 1995, A&A, 293, 87
 Koch D. G. et al., 2010, ApJ, 713, L79
 Mackey A. D., & Broby Nielsen P., 2007, MNRAS, 379, 151
 Miglio A. et al., 2009, A&A, 503, L21
 Miglio A., 2011, arXiv:1108.4555
Miglio A. et al., 2012, MNRAS, 419, 2077
 Milone A. P., Bedin L. R., Piotto G., & Anderson J. 2009, A&A, 497, 755
 Mosser B. et al., 2010, A&A, 517, 22

- Pols O. R., Tout C. A., Eggleton P. P., Han Z., 1995, *MNRAS*, 274, 964
- Pols O. R., Schroder K. P., Hurley J. R. Tout C. A., Eggleton P. P., 1998, *MNRAS*, 298, 525
- Reimers D. 1975, *Memoires of the Societe Royale des Sciences de Liege*, 8, 369
- Rocha-Pinto H. J., Maciel W. J., Scalo J., Flynn C., 2000, *A&A*, 358, 850
- Rubele S., Girardi L., Kozhurina-Platais V., Goudfrooij P., Kerber L., 2011, *MNRAS*, 414, 2204
- Salpeter E. E., 1955, *ApJ*, 121, 161
- Schröder K. P., Pols O. R., Eggleton P. P., 1997, *MNRAS*, 285, 696
- Stello D., Chaplin W. J., Basu S., Elsworth Y., Bedding T. R., 2009a, *MNRAS*, 400, L80
- Stello D. et al., 2009b, *ApJ*, 700, 1589
- Stello D. et al., 2010a, *ApJ*, 713, L182
- Stello D. et al., 2010b, *AN*, 331, 985
- Stello D. et al., 2011, *ApJ*, 739, 13
- Ulrich R. K., 1986, *ApJ*, 306, L37
- Yang W., Bi S., 2007, *A&A*, 472, 571
- Yang W., Li Z., Meng X., Bi, S., 2011a, *MNRAS*, 414, 1769
- Yang W., Meng X., 2009, *PASJ*, 61, 1399
- Yang W., Meng X., 2010, *New Astron.*, 15, 367
- Yang W., Meng X., Bi, S., Tian, Z., Li, T., Liu, K., 2011b, *ApJ*, 731, L37
- Yang W., Meng X., Li Z., 2010, *MNRAS*, 409, 873